Biosensors and Bioelectronics 130 (2019) 352–359

Contents lists available at ScienceDirect

Biosensors and Bioelectronics

journal homepage: www.elsevier.com/locate/bios

Reduced graphene-oxide transducers for biosensing applications beyond the Debye-screening limit

Xiaoling Lu[a,b], Anna Miodek[c], Walid-Madhat Munief[b], Pawan Jolly[c,1], Vivek Pachauri[a,b], Xianping Chen[d], Pedro Estrela[c], Sven Ingebrandt[a,b,*]

[a] Institute of Materials in Electrical Engineering 1, RWTH Aachen University, Aachen, Germany
[b] Department of Informatics and Microsystem Technology, University of Applied Sciences Kaiserslautern, Zweibrücken, Germany
[c] Centre for Biosensors, Bioelectronics and Biodevices (C3Bio) and Department of Electronic and Electrical Engineering, University of Bath, Bath, United Kingdom
[d] Key Laboratory of Optoelectronic Technology & Systems, Education Ministry of China and College of Optoelectronic Engineering, Chongqing University, Chongqing, China

ARTICLE INFO

Keywords:
Reduced graphene-oxide thin films
In-line electrochemical impedance spectroscopy
Aptasensor
Debye-screening limitation

ABSTRACT

In the field of label-free biosensing, various transducer materials and strategies are under investigation to overcome the Debye-screening limitation of charged biomolecules. We demonstrate an in-line, impedimetric aptasensor with reduced graphene-oxide (rGO) thin films as transducers to detect prostate specific antigens (PSA) in a physiological buffer solution. Unlike classical electrochemical impedance spectroscopy (EIS), this direct, label-free and fully-electronic biosensor approach does not need any redox markers. As specific capture molecules, short anti-PSA aptamers ensured a close binding of the target molecules to the transducer surfaces. Results showed a limit of detection smaller than 33 pM of PSA and a wide detection range from 0.033 to 330 nM fully covering the clinically relevant range of PSA (0.115–0.290 nM). This promising performance can be attributed to the bipolar electronic transport characteristics of the ultra-thin rGO layers similar to pristine graphene. The attachment of target biomolecules to the films changes the resistance of the rGO thin films. Such an in-line EIS configuration with rGO thin films opens promising prospects for biosensing beyond the Debye-screening limitation, which is a major challenge for conventional semiconductor field-effect devices towards clinical applications.

1. Introduction

Electrochemical impedance spectroscopy (EIS) (Orazem and Tribollet, 2011; Lisdat and Schafer, 2008; Barsoukov and Macdonald, 2005; Macdonald, 2005; Macdonald, 1990) is widely used as a sensitive, selective and label-free biosensing principle to analyze biorecognition events on sensor surfaces. The technique extracts the complex impedance of a system under test by applying an alternating voltage perturbation of small amplitude (generally mV) in a certain frequency band while measuring the current response. Conventional EIS can be classified into faradaic and non-faradaic modes. Faradaic EIS measurements are usually done in the presence of redox molecules and the amount in redox current varies with the electronic property of the working electrode. When biomolecules are binding to these electrodes, their accessible surface gets smaller and hence the redox current is reduced. The current decrease can then be related to the receptor-analyte binding at the surface and concentrations of analyte molecules can be measured. The total faradaic current also strongly relies on the electronic properties of the biomolecules, since some of the biomolecules can be redox-active, while most of the biomolecules act as an insulating layer.

For the non-faradaic EIS, the impedance measurement is carried out in absence of redox molecules (Bart et al., 2005). A classical device configuration are interdigitated electrodes (IDEs), which are described as capacitive biosensors (Berdat et al., 2008, 2006; Yang et al., 2004). They are known to exhibit a high sensitivity due to the local confinement of the electrical field in the micrometer-size IDEs structures. In both faradaic and non-faradaic EIS, conventional impedance measurements are detecting impedance changes of the biosystem between counter and working electrode by passing current through the buffer solution on top of them. Advanced transducer layers can be additionally applied in between the IDE finger electrodes and the biorecognition layer to amplify the output signals and to enhance the sensitivity of the sensors. In many cases, this improvement stems from a higher density of

* Corresponding author at: Institute of Materials in Electrical Engineering 1, RWTH Aachen University, Aachen, Germany.
E-mail address: ingebrandt@iwe1.rwth-aachen.de (S. Ingebrandt).
[1] Present address: Wyss Institute for Biologically Inspired Engineering at Harvard University, Harvard Medical School, Boston, USA.

https://doi.org/10.1016/j.bios.2018.09.045
Received 1 July 2018; Received in revised form 1 September 2018; Accepted 12 September 2018
Available online 14 September 2018
0956-5663/

the bio-recognition molecules on the sensor surfaces.

In recent years in the field of biosensor and bioelectronics, chemically exfoliated graphene oxide (GO) and reduced graphene oxide (rGO) attracted lots of attention due to its similarity to pristine graphene. Graphene (Novoselov et al., 2004, 2012; Castro Neto et al., 2009; Geim and Novoselov, 2007; Kahng et al., 2012; De and Coleman, 2010; Baringhaus et al., 2014; Huang et al., 2011) is an atomic 2D material and consists of a carbon hexagonal lattice that possesses high carrier mobility, excellent mechanical properties, high thermal stability and good biocompatibility. GO (Dreyer et al., 2010; Eda and Chhowalla, 2010) and rGO (Bagri et al., 2010; Gómez-Navarro et al., 2007; Pei and Cheng, 2012) thin films not only preserve this carbon lattice alike graphene to maintain the above-mentioned, promising properties within nanoscale, but also own various functional oxygen groups on their carbon basal plane. This is beneficial for chemical attachment of capture molecules to the thin films. Therefore, these two materials are intensively studied as alternatives to overcome the dilemma that graphene is facing towards its wafer-scale fabrication and process integration (Suk et al., 2011; Liang et al., 2011). In most of the cases, rGO thin films (Bonanni et al., 2012b, 2012a) are utilized as transducer layers in conventional, faradaic EIS to enhance the sensing area by the various functional oxygen groups on its basal plane.

In the present study, an in-line EIS biosensor platform was developed with rGO thin films as transducer layers on top of IDEs (Zaretsky et al., 1988; Igreja and Dias, 2004), while the impedance was measured along the rGO thin film. This transducer principle is label-free does not need redox markers. Since in this configuration the IDE electrodes are bridged by a conductive material, already at low frequencies (1 Hz) significant changes in the impedance values upon biomolecule binding are visible. The promising semi-metal properties of rGO with a strong reaction to surface potential changes were advantageous for biosensing. In addition a short, 32 base pair anti-PSA aptamer sequence as ultra-thin biorecognition layer (Jolly et al., 2015; Formisano et al., 2015) facilitated the detection of PSA in physiological buffer concentrations. The electronic signal confinement at the IDE sensor spots for both rGO thin films and IDEs demonstrate a precedential biosensing capability beyond the typical Debye-screening limit in aqueous solutions. Our study is presenting a proof-of-concept towards a later application of the rGO platform to detect cancer-related biomarkers directly from human patient samples.

2. Materials and methods

2.1. Chemicals and reagents

Amine-terminated, PSA-specific DNA aptamer (5′-NH_2-$(CH_2)_6$ –TTTT TAAT TAAA GCTC GCCA TCAA ATAG CTTT-3′) and (3-Aminopropyl) triethoxysilane (APTES) were purchased from Sigma Aldrich, Germany. PSA was obtained from Merck Chemicals Ltd. (Beeston, UK). For the electronic assays, 10 mM phosphate-buffered saline (PBS) with pH 7.4 was used. This PBS buffer solution consisted of 10 mM phosphate buffer (pH adjusted from a mixture of monohydrate phosphate and dinatrium hydrogen phosphate), 2.7 mM KCl and 137 mM NaCl having a physiological saline concentration similar to human blood serum. Other chemicals for biofunctionalization and biosensing experiments as mentioned in the following were purchased from Sigma Aldrich and used without further purification.

2.2. Preparation of GO flakes

GO flakes were chemically exfoliated by a recently described Low-temperature exfoliation and desalinization (LTEDS) method. The synthesis and characterization of this base material and its integration into a routine clean room process were described in an earlier publication (Lu et al., 2018). In short, graphite powder (Alfa Aeser, natural, - 325 mesh, 99.8%) was fully oxidized and exfoliated in a reflux condenser with a mixture of H_2SO_4 and H_3PO_4. To ensure a mild exfoliation but not slow down its speed, the reaction temperature was stabilized by a cooling water flow system to 20 °C. Subsequent to the reaction, the mixture was quenched with ice water mixed with H_2O_2 (100:1 vol%). The obtained GO solution was filtered through a stainless steel sieve (200 µm, Spoerl OHG) lined with a polyester fiber. It was essential to eliminate all ionic products Mn^{2+}, SO_4^{2-}, PO_4^{3-} and K^+ out of the dispersion, which was realized with a dialysis membrane (Th. Geyer GmbH & Co.KG). Dialysis was repeated twice to avoid ion inclusions. Afterwards, the dialyzed GO dispersion was mixed with DI water and 3× centrifuged until the last supernatant reached at pH value of 2.0. Furthermore, the GO mass was mixed with HCl and centrifuged, followed by 2× centrifugation in ethanol. Each centrifugation step was followed by GO solution filtering with the polyester fiber sieve. The obtained residue was coagulated with diethyl ether and filtered through a sieve lined with a PTFE filter (mesh size 0.45 µm). The filtered graphene oxide solution was evacuated for 2 days inside a desiccator to dry it. The lateral sizes of the resulting flakes ranged from 300 nm to 20 µm due to eventual aggregation of the GO material in the sieve. To obtain lateral mono- and multi-layer GO flakes, the dispersion was centrifuged again until a final pH value of 2.9 was reached. The resulting GO material was water soluble and could be applied in the next steps as spin-coating solution to form ultra-thin GO films.

2.3. Fabrication of GO thin films and devices

In the present study, the GO thin films were prepared on 4-in. wafers in a routine clean room process. Glass or SiO_2/Si wafers were thoroughly cleaned with freshly prepared Caro's acid (H_2O_2 and azeotropic H_2SO_4; ratio 1:3). Afterwards, the wafers were activated by an O_2 plasma (t = 5 min, 230 W) and functionalized by APTES in a gas-phase silanization process (Munief et al., 2018a). In this process, the terminal -OH groups of the activated silicon oxide surface are replaced by O-CH_2-CH_3 ethoxy-groups in a S_N1 reaction scheme (Schmitt, 2014; Schmitt et al., 2015). In a parallel work, we optimized this procedure using a gas-phase silanization approach and we characterized the thin siloxane films by various surface characterization methods in detail Munief et al. (2018a). During the surface reaction, an ultra-thin 3-Aminopropylsiloxane (APS) layer is formed on the wafer surface. The high quality and homogeneity of these APS coatings form the basis of the robust, uniform and ultra-thin reduced graphene oxide films, which can be readily integrated into a full wafer fabrication protocol as we described it in an earlier publication (Lu et al., 2018). After the APS coating, the wafers were washed with ethanol. The -NH_2 groups of the APS layer can covalently bind the GO flakes by reacting with their -COOH groups. 5 ml GO solution $pH = 2.9$ was applied and spin-coated onto the wafer surface. A more detailed process description can be found in our previous publication (Lu et al., 2018).

2.4. Thermal reduction of GO devices

The prepared GO devices were placed inside a vacuum oven (VT5042 EKP, Heraeus, Germany) at 350 °C for 10 h to remove the oxygen functional groups and to reduce the material gradually. Afterwards, to generate ohmic contacts between the thin films and the Au electrodes underneath, the devices were rapidly annealed in a high temperature oven (DS-3900-PC-150, INOTHERM, Germany) at 600 °C for 20 s in ambient air. GO flakes inside a film are then reduced to rGO and the network of flakes forms a quilted layer with bipolar electronic transport properties similar to pristine graphene, but with much smaller carrier mobilities.

2.5. rGO thin film based in-line EIS configuration

The rGO IDEs devices were fabricated in the clean room of the University of Applied Sciences Kaiserslautern at Zweibrücken campus,

Germany. IDEs were primarily prepared on 4-in. glass wafers by standard photolithography (MA/BA 6, Süss, Germany), metal evaporation (BAK500, Oerlikon Balzers, Liechtenstein) and lift-off processes. The electrode material was a bilayer stack of 270 nm Au and 30 nm Ti as adhesion layer to the glass. Overall, the 4-in. wafer design included 72 chips with a size of $7 \times 7\ mm^2$. Each chip contained a 4×4 array with 16 individual drains sharing a common source electrode. The resistance and capacitance of each drain electrode was designed to be equal for accurate comparison of measurement results between the 16 channels. The widths and lengths of the drain electrodes were 5 μm and 100 μm, respectively, while the separation distance of the neighboring electrodes was 5 μm. For 10 electrode fingers, IDEs had an effective channel length of 900 μm. The GO thin film was formed on top of already prepared IDEs using spin-coating. This procedure forms ultra-thin but uniform GO films in the range of 1.5–2 nm per spin coating step (Lu et al., 2018). In total six spin-coating steps were applied for the devices used here in order to ensure complete films without defects resulting in about 8 nm thickness. For patterning of the GO thin films, we applied standard photolithography. Afterwards, the films were protected by photoresist and the unprotected areas were etched away by O_2 reactive ion etching (SI 591M, SENTECH, Germany).

2.6. Biofunctionalization of the rGO IDEs

The biofunctionalization procedure for the aptamer receptor layer was as following: 80 mM N-(3-Dimethylaminopropyl)-N′-ethylcarbodiimide hydrochloride (EDC) was mixed with 20 mM N-Hydroxysuccinimide (NHS) in milliQ water (resistivity 18.2 MΩ·cm) and used to activate the -COOH groups on the surface of the rGO thin films for a covalent immobilization of the amino-terminated aptamers. 100 μL of EDC/NHS solution was applied on the rGO thin films for 30 mins at room temperature. For an optimum conformation to capture the PSA molecules the aptamers were treated as following: Microcentrifuge tubes containing 10 μL of 100 μM aptamers were defrosted at ambient conditions and fast spinning was used to collect the residual droplets on the tube's sidewall. Then the microcentrifuge tubes were immersed into 90 °C hot milliQ water. After cooling down to room temperature, the microcentrifuge tubes were again centrifuged. The 100 μM amino-terminated aptamers were diluted to 2 μM by 10 mM PBS with a final pH value of 7.4. 100 μL of 2 μM aptamer solution was then applied on the rGO thin films for 30 mins at room temperature immediately after their EDC/NHS activation and then left at 4 °C overnight. For the next step the chips were washed with PBS and a blocking solution of 1 mM ethanolamine (pH = 8.5 prepared with PBS) was applied for 30 mins. This blocking procedure saturated the remaining -COOH groups of the rGO thin films and suppressed the non-specific binding. The different concentrations of PSA for the calibration curve were prepared by stepwise diluting 100 μM stock solution in 10 mM PBS. The dose-response measurements started by incubating the chips in 100 μL PSA with a concentration of 33 fM for 30 mins. After each step, the chips were washed with 10 mM PBS and the in-line EIS spectra were recorded using an impedance analyzer (Ivium COMPACTSTAT.e, Ivium Technologies, Netherland). In total eight concentrations of PSA were used: 33 fM, 330 fM, 3.3 pM, 33 pM, 330 pM, 3.3 nM, 33 nM and 330 nM.

2.7. Control experiments with Human Serum Albumin (HSA)

To check the specificity of the rGO biosensors, the sensor surface was prepared similarly to the protocol described in Section 2.6 but without the aptamer immobilization. A highly concentrated stock solution of 100 μM human serum albumin (HSA) was prepared in 10 mM PBS (pH~7.4) and subsequently filtered by a filter with pore size of 0.2 μm. The test solution of 1 μM HSA was prepared by diluting the 100 μM stock solution in 10 mM PBS (pH~7.4). In the control experiments, this non-specific solution was applied similarly to the PSA solutions.

2.8. Fluidic setup

A fluidic setup was printed by a 3D printer (Objet350 Connex, Stratays Ltd., Israel). It contained a top and a bottom part. The top part had a container in its center and a sealing rubber ring at the side. The IDE rGO sensor chips were clamped between these two parts, while the rGO arrays were exposed to the liquid. Details of this measurement cell were described earlier (Lanche et al., 2014). All of the surface functionalization and sensor measurements were carried out within this fluidic cell.

2.9. Measurement setup

For the in-line EIS experiments the two arms of the IDEs acted as working electrode (WE) and counter electrode (CE), respectively, while an electrochemical Ag/AgCl electrode (DRIREF-2SH, WPI, Germany) served as reference electrode (RE). This configuration is denoted as in-line EIS in the following. The electronic performance of the rGO IDE sensors were compared in 10 mM PBS buffer solution under the following conditions: the DC offset potential and AC signals were applied to the WE and CE, repectively, against a constant potential at the RE (the standard potential of the Ag/AgCl electrode is 0.23 V in 3 M KCl at room temperature). An equilibration time of 30 s was allowed before the impedance spectra were recorded. The DC potential offset was 50 mV while the AC stimulation voltage was 10 mV in amplitudes. The frequency range was scanned from a high frequency of 100 kHz to a low frequency of 0.1 Hz. The alternating current output I_{out} (t) flowing from the WE to the CE was recorded by the impedance spectrometer. The 10 mM PB test solution was prepared by dissolving PB tablets in highly pure milliQ water (resistivity 18.2 MΩ cm) with a final pH value of 7.4.

3. Results

We established an aptasensor platform with rGO thin films as transducer layers on top of IDEs to detect PSA. The biosensor devices were measured in an in-line EIS configuration in 10 mM PB buffer solution (ionic strength 162 mM), which determines a Debye screening length of the biomolecule charges 0.76 nm. In our dose-response experiments we found that the rGO based aptasensor exhibit a sensing capability beyond the Debye-screening limit, as well as a wide sensing range covering the clinically relevant concentration range of PSA.

3.1. rGO-IDEs device

Our devices consist of ultra-thin rGO films, which are quilted layers of small GO flakes structured on top of 16-channel IDEs arrays on glass wafers. Graphene oxide flakes were chemically exfoliated by the LTEDS method and spin-coated on top of APTES-functionalized wafer surfaces with pre-fabricated IDEs arrays (Lu et al., 2018). The spin-coating procedure is forming uniform thin films, which were subsequently patterned into microstructures by standard photolithography and O_2 plasma etching. A scanning electron microscopy (SEM) image of an exemplary rGO IDEs electrode structure is shown in Fig. 1**A**. The thickness of the GO patterns was measured by atomic force microscopy (AFM) and was 8 nm as shown in Fig. 1**B**.

3.2. Electronic performance of the rGO based in-line EIS

In the present study, EIS measurements were done in an in-line impedance configuration as schematically shown in Fig. 2. The two arms of the IDE structures and the Ag/AgCl electrode served as working (WE), counter (CE) and reference (RE) electrodes, respectively. A sinusoidal voltage V_{in} (t) input was applied to the WE, which changes its potential relative to the fixed potential of the RE. The alternating

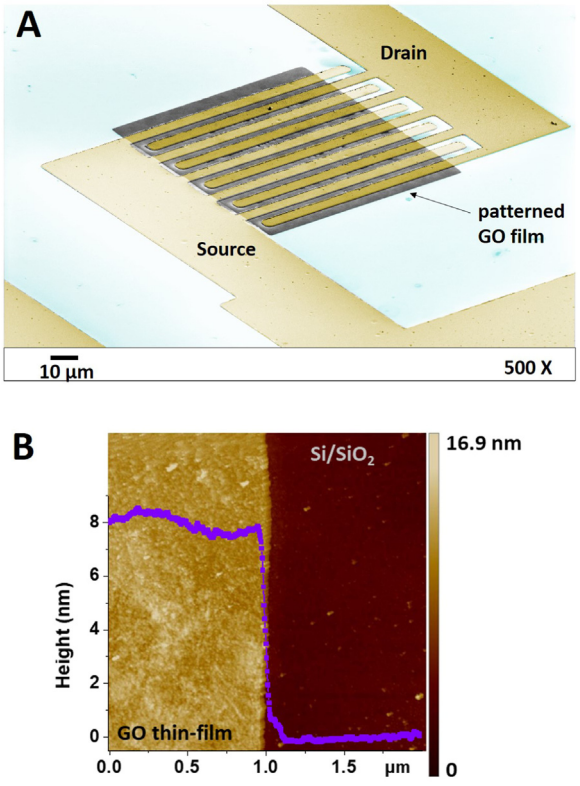

Fig. 1. Characterization of GO thin films: (A) Scanning electron microscopy image of an GO thin-film patterned on top of interdigitated gold microelectrodes (IDEs). (B) Atomic force microscopic image of a GO thin-film at the edge of a structured pattern. The step size shows a film thickness of 8 nm with a smooth GO surface.

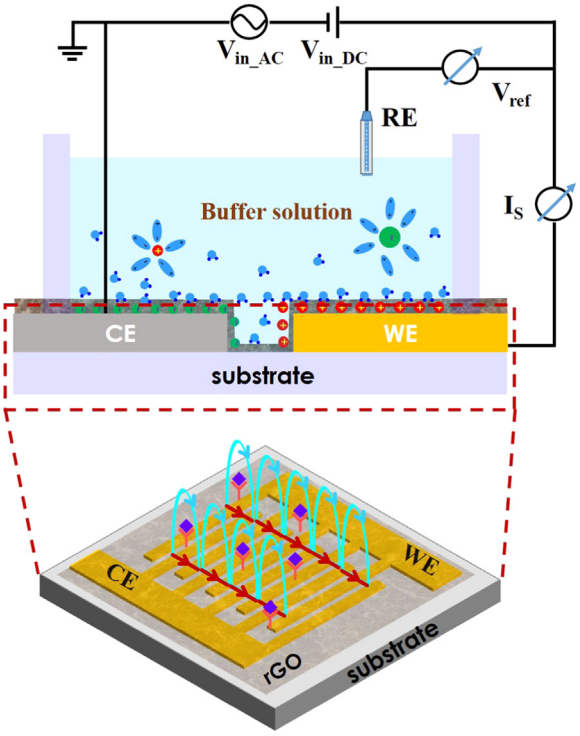

Fig. 2. In-line EIS configuration of the rGO IDE biosensors: The two arms of the IDE structures and an electrochemical Ag/AgCl electrode serve as working electrode (WE), counter electrode (CE) and reference electrode (RE), respectively.

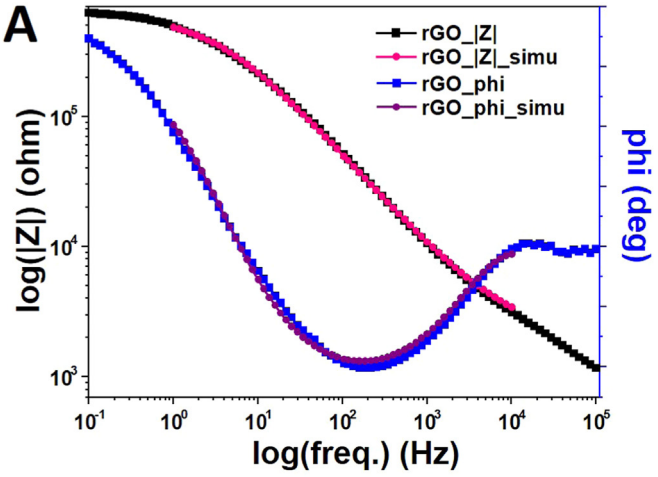

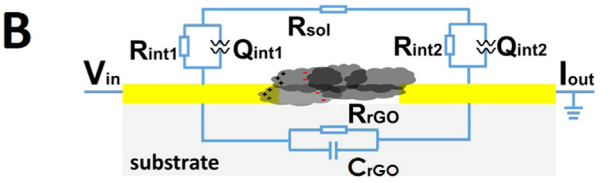

R_{rGO}	900 kΩ	R_{int1}	9.84×10^{-7}	R_{int2}	2.196×10^{-7}
C_{rGO}	1.37 nF	Q_{int1}	1.2×10^{-6}	Q_{int2}	1.2×10^{-6}
R_{sol}	2830 Ω	n_{int1}	0.7	n_{int2}	0.718

Fig. 3. Electronic characterization of an rGO IDE sensor in an in-line EIS configuration: (A) Experimental and simulated Bode plots of an in-line EIS spectrum measured in 10 mM PBS solution. (B) Equivalent circuit for the rGO IDEs: $R_{int1(2)}$ and $Q_{int1(2)}$ are the resistance and CPEs of the EDLs, respectively. R_{sol} is the resistance of the electrolyte solution. R_{rGO} and C_{rGO} are the resistance and the capacitance of the rGO thin film, respectively. Value of the equivalent circuit elements obtained from the fit are listed in the table.

output current I_{out} (t) between WE and CE was recorded. The quotient of V_{in} (t)/I_{out} (t) is marked as impedance Z of the IDE sensor.

In our measurements we used an input voltage V_{in} (t) of 10 mV amplitude in a frequency range from 0.1 Hz to 100 kHz, while a DC bias voltage of 50 mV was applied. A typical Bode plot of the rGO in-line EIS is shown in Fig. 3**A**. In the quilted rGO thin film, the overlapping regions of neighboring rGO flakes bridge the path and meanwhile constrain the direction of the carrier transport inside the thin film. An electronically equivalent circuit of the rGO thin film can be composed of a resistor R_{rGO}, representing the current transport inside the rGO flakes, in parallel with a capacitor C_{rGO}, representing the capacitive flake-to-flake transport. The current from the WE to the CE arm of the IDE could either pass through the electrochemical double layers (EDLs) at the electrode contacts in series with the solution resistance R_{sol} or through the rGO thin film with the R_{rGO} and C_{rGO} elements in parallel. The EDL is not an ideal capacitor and is represented by a CPE for both WE and CE. By considering the resistance and capacitance of the rGO thin films into pre-developed circuits for bare IDE biosensors (Berdat et al., 2008), an equivalent circuit for our rGO in-line EIS can be extracted as indicated in Fig. 3**B**.

3.3. PSA biosensing by rGO based in-line EIS

We used a highly-specific aptamer sequence (TTT TTA ATT AAA GCT CGC CAT CAA ATA GCT TT from 5′ to 3′) for PSA detection. The very good sensitivity and also the highly-specific response of this

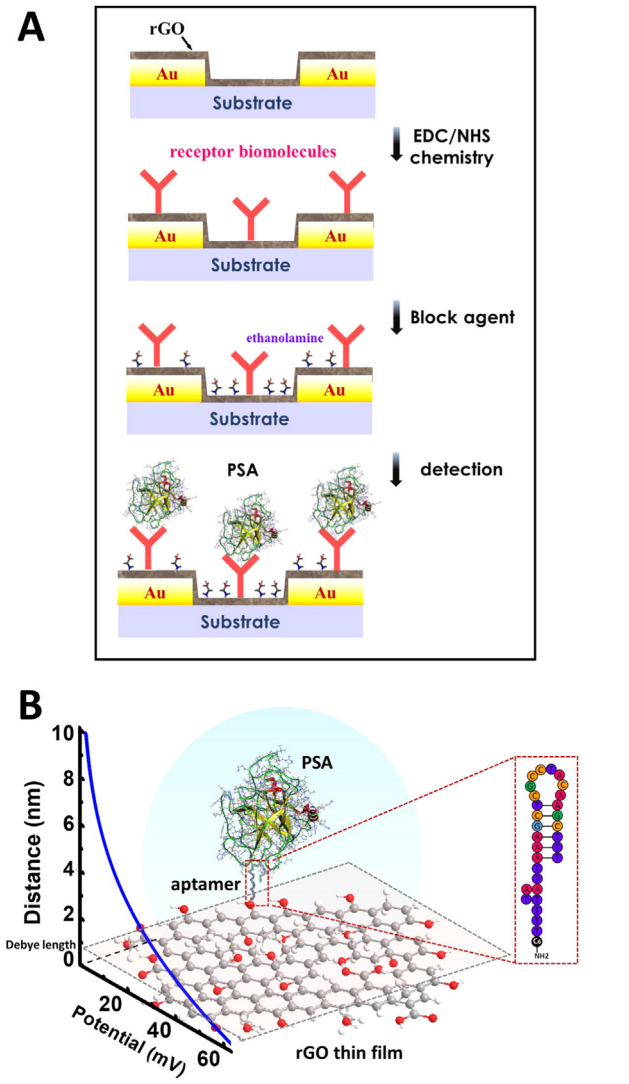

Fig. 4. Descriptive schematics of the rGO IDE EIS experiments to detect PSA: (A) Preparation flow of the aptasensor platforms: The -COOH groups on the surface of the rGO thin films were activated by standard EDC/NHS chemistry, such that the amino-terminated receptor biomolecules can be covalently immobilized. Afterwards, the surface was saturated by ethanolamine to suppress non-specific binding. In the following, PSA was detected. (B) Descriptive schematics of an rGO IDE biosensor with aptamer receptor biomolecules, which locates outside the Debye-screening length (0.76 nm) on the rGO transducer layer.

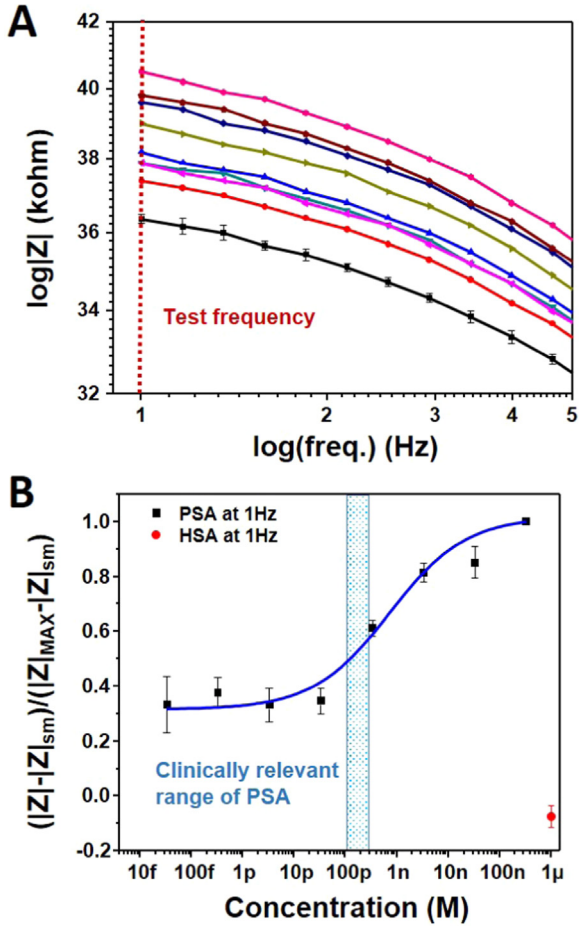

Fig. 5. Dose-response experiment to extract a calibration curve for PSA detection: (A) The impedance amplitudes at low frequencies (1–5 Hz) are strongly influenced by the biomolecule binding. (B) Amplitude calibration curve of the PSA dose-response experiments. 1 μM human serum antigens (HSA) were used as a non-specific control (red data point at the right bottom of the graph). (For interpretation of the references to color in this figure legend, the reader is referred to the web version of this article.)

receptor layer was already presented in earlier works (Jolly et al., 2015; Formisano et al., 2015). The 5′ end of the aptamers is modified by a 6-carbon chain as a spacer and terminated with an amino group for covalent tethering to the sensor surface. Ethanolamine (10 mM) was used to block the remaining -COOH groups on the biosensor surface. The schematic of the biosensor surface functionalization protocol is shown in Fig. 4**A**. The Debye-screening length in the 10 mM PBS solution is only 0.76 nm. The aptamer size is approximately 3–5 nm for a fully stretched molecule. Upon folding into the 3D aptamer structure this size should be smaller. The target molecule PSA is of 33 kDa molecular weight and its diameter is approximately 4.5 nm. The depictive schematic with folded aptamers as receptor biomolecules to detect PSA on rGO thin film is shown in Fig. 4**B**

Dose-response experiments were done in a full frequency range from 0.1 Hz to 100 kHz. A bode plot of the full spectra is shown in the Supporting information S1. A close-up of the impedance amplitude at the low frequency range 1–5 Hz is given in Fig. 5**A**. A calibration curve for PSA detection was composed from the impedance amplitudes at 1 Hz as shown in Fig. 5**B**. Five channels are summarized and small error bars indicate a very reproducible sensor response. A control experiment with a high concentration of HSA showed no response (compare individual data point in Fig. 5**B**), demonstrating a highly specific detection of PSA.

4. Discussion

World-wide prostate cancer is one of the leading causes of the cancer-related death in men (Baade et al., 2009). As a most common representative biomarker, PSA is used to address the presence of prostate cancer and to identify the relapse after receiving the cancer treatment (Antenor et al., 2005). To detect PSA, plenty of efforts are dedicated to exploit the biosensing capability of various nano-/micro-devices to achieve a perfect biosensor: highly selective, robust, reliable, cost-effective, disposable, environmentally friendly, portable towards point of care usage, with an optimized response to cover the clinically relevant concentration range of PSA. The currently available, label-free biosensors for quantitative detection of PSA severely encounter the Debye-screening limitation in physiological matrices.

In this study, we developed an aptasensor with rGO thin films as transducer layers in an in-line EIS device configuration and we tested this biosensor platform to detect PSA in similar ionic strength as

physiological matrices. The PSA dose-repose experiments demonstrated a biosensing capability beyond the Debye-screening limitation. This result was confirmed by dose-response experiments of I-V dual sweep, which provide additional proof (Supporting information S2).

All rGO-IDE devices used in this study were prepared on a 4-in. wafer from the same fabrication bench. The chemical exfoliation procedure to generate GO aqueous solution, various characterizations of the GO material, the preparation flow for the GO and rGO thin films and the device fabrication were detailed in our previous publication (Lu et al., 2018). In the present work, the GO aqueous solution was spin-coated on IDEs structure multiple times to form GO thin films, which are complete without pinholes and which are topographically uniform. With a thermal reduction protocol GO thin films were transformed into conductive rGO thin films. Thin films patterned on top of the IDE structures had a thickness of 8 nm.

In order to take advantage of the biosensing capability of the rGO thin films in their lateral direction, in-line EIS measurements were done (Fig. 2). Already at small frequencies of 1 Hz the responses were stable and showed a reliable biosensor readout. Mathematically, the impedance Z is expressed either in its polar form $Z = |Z|e^{j\varphi}$ or in the Euler's form $Z = Z_1 + jZ_2$ which correspond to Bode plot and Nyquist plot, respectively. In our study, Bode plots were used to analyze the data. The equivalent circuit as shown in Fig. 3B can be used to simulate the Bode plots. The current flow inside the quilted rGO layers can be described by a resistor R_{rGO} in parallel to a capacitor C_{rGO}. The capacitance behavior of the rGO thin film was also proven by C-V measurements in dry state (Supporting information S3). In these measurements, the rGO thin film clearly formed ohmic contacts with the IDEs, but were acting as capacitors under AC stimulation. For the current flow through the buffer solution on top of the IDEs, the equivalent electrical circuit of the two EDLs composed of a resistor and a constant phase element (the CPE is defined by its exponent n (dimensioless) and factor Q (in units s^n/Ω) with an impedance of $Z = 1/(j\omega Q^n)$) in parallel and both in series with the solution resistance R_{Sol}. To model this solid-liquid interface and to prove that a CPE needs to be included for this part of the circuit we did classical out-of-line EIS experiments in addition (Supporting information S4). From these measurements we can extract the equivalent circuit elements of the EDLs at the interface of the rGO thin films and the buffer solution. We confirmed that a CPE needs to be used for this part. Based on the equivalent circuit model shown in Fig. 3B the following parameters can be extracted from the simulation: $R_{rGO} = 900\ k\Omega$, $C_{rGO} = 1.37\ nF$, $R_{sol} = 2830\ \Omega$, $R_{int1} = 9.84\times10^{-7}\ \Omega$, $Q_{int1} = 1.2\times10^{-6}$, $n_1 = 0.7$. $R_{int2} = 2.196\times10^{7}\ \Omega$, $Q_{int2} = 1.2\times10^{-6}$, $n_2 = 0.7$,

with $R_{int1,2}$ and $Q_{int1,2}$ the resistors and CPEs and $n_{1,2}$ the CPE factors of the IDE arms in contact with the test solution.

An aptamer usually consists of a short, single-stranded DNA sequence and its specific conformation provides a high affinity towards a target biomolecule. The structure of the anti-PSA aptamer used in our study is forming a hairpin loop, because two regions of the stand are complementary and form local Watson-Crick base pairs (Fig. 3B). In this configuration the aptamer size is about 3–5 nm. The molecular weight of PSA is 33 kDa and its diameter is approximately 4.5 nm.

The PSA detection was done in 10 mM PBS solution with an ionic strength 162 mM and a Debye-screening length of 0.76 nm. The Debye length depends on the solvent permittivity $\varepsilon_s = \varepsilon_0\varepsilon_r$, number concentrations of the solute ions $n_{i\infty}$ ($/m^3$) and valence of the solute ions Z_i by the following Eq. (1):

$$\kappa^{-1} = \sqrt{\frac{\varepsilon_s k_B T}{\sum_i n_{i\infty} Z_i^2 e^2}}, \quad (1)$$

in which $\varepsilon_0 = 8.854\times10^{-12}\ F\ m^{-1}$ is the vacuum permittivity, $\varepsilon_r = 78$ is the relative permittivity of water, $k_B = 1.38\times10^{-23}\ J\ K^{-1}$ is the Boltzmann constant, T = 300 K is the room temperature, $e = 1.602\times10^{-19}$ C is the charge of an electron, the ion number $n_{i\infty}$ = molar concentration × N_A, Avogadro constant $N_A = 6.02\times10^{-23}\ mol^{-1}$. In terms of the Debye-screening mechanism, this measurement condition is very similar to physiological solutions. In this condition, a typical field-effect based semiconductor biosensor will hardly show any sensing due to the Debye-screening of charges. The bound PSA biomolecules are located outside the EDL due to their larger sizes compared to the Debye length. Therefore, their charges should not be able to modulate the current inside a semiconductor transistor channel.

In contrast to this, the rGO IDE based in-line EIS biosensors exhibit a very promising sensing performance beyond this Debye-screening limit. The impedance amplitude at low frequencies clearly increases with increasing concentration of PSA (Fig. 5A). A non-specific control experiment HSA was used in a high concentration of 1 μM. The specific signals corresponding to the PSA binding can be clearly distinguished from this non-specific control (Fig. 5A, red data point). As it can be seen from the calibration curve depicted in Fig. 5B, the limit of detection of the rGO IDE biosensor platform was about 33 pM. In this plot, the clinically relevant concentration range is marked (4–10 ng/ml corresponding to 115–290 pM.) and it can be seen, that the biosensor perfectly matches this range with highest signal resolution there.

As an alternative transducer mechanism, we also analyzed the biorecognition capability or the aptamer receptor layer by dual I-V sweeps in an ion-sensitive field-effect transistor (ISFET) configuration. The obtained results (Supporting information S2) confirm as well that the PSA binding leads to an increase of the rGO thin film resistance. This coincides with the results from the in-line EIS configuration. It is obvious from our results that the rGO thin films can respond to binding of PSA biomolecules even though the geometrical situation at the surface should not allow for charge sensing in physiological buffers. Eventually, the binding leads to a disturbance of the EDL on top of the rGO material. In the electrolyte-gate field-effect configuration, this EDL is forming the 'gate dielectrics' of the transistor. The tendency of the observed resistance increases can be explained by the bipolar transport properties of the rGO thin films (Fig. S4B-C).

PSA is negatively charged in 10 mM PBS at pH 7.4 due to its isoelectric point of 6.9-7.2, depending on the glycosylation level. The attachment of PSA onto the rGO thin films is equivalent to an additional negative voltage. The Dirac points in the bipolar curves were shifted to the left compared to $V_{GS} = 0$. Therefore we can conclude that the rGO was initally n-doped. The negative voltage that is caused by the PSA attachment modifies the Fermi level and the carrier concentration within the rGO. The binding of more PSA molecules leads to a higher negative voltage applied across the rGO thin film. Therefore, the conductivity of the rGO channel decreases and its resistance increases. This could explain the results obtained in our in-line EIS and in the dual I-V sweep experiments for PSA detection.

5. Conclusions

We used ultra-thin, conductive rGO films structured on top of micro-sized IDE arrays as transducer layers to detect PSA. Highly specific and small-size aptamer sequences were used as receptor layer and an in-line, electrochemical impedance spectroscopy configuration showed specific biosensor responses at low frequencies. All experiments were done in 10 mM PBS corresponding to an ionic strength of 162 mM and hence a Debye-screening length of only 0.76 nm. In terms of the detection mechanism, this test solution is very similar to typical physiological solutions such as blood serum. Impedance amplitudes at low frequencies (1–5 Hz) showed a highly sensitive response and the concentration range covered 0.033–330 nM. We demonstrated that our rGO thin films preserve a bipolar transport property similar to graphene with the clear advantage that this material can be integrated into a standard process flow on wafer scale. The binding of PSA biomolecules increased the rGO channel impedance at low frequencies (i.e. resistances). This tendency was confirmed by I-V sweeps in an ISFET configuration, which showed similar resistance changes. The established rGO biosensor platform can detect PSA fully covering its

clinically relevant range (4–10 ng/ml) in physiological buffer concentrations.

In a recently published study, we used the same aptamer sequence to detect PSA on a silicon nanowire (SiNW) array platform. There we found a similar limit of detection below 50 pg/ml, but the response in the clinically relevant concentration range was not optimum, since the devices reached a saturation at low concentrations already (Rani et al., 2018). Compared to the SiNW platform, the rGO IDE devices as introduced in this study are much easier to fabricate and are therefore much more promising towards eventual commercialization.

Although we confirmed the sensing mechanism and the capability to detect PSA in a physiological buffer solution, for real clinical applications additional steps are necessary. In the next phase of our project, the experiments need to be done in human serum to prove the specificity of the aptamer receptor layer. In a parallel work, we confirmed that the rGO layers are stable in a human serum and an antibody/antigen immunoassay showed specific responses (Munief et al., 2018b). In this other work we used an ISFET configuration for the rGO sensors and the binding of N-terminal pro brain natriuretic peptides, a cardiac inflammation marker, caused an increase of the rGO layer resistance. This is a very similar response compared to the PSA assays presented in this study. Therefore, we are fully convinced that our rGO biosensor transducer layers are a promising tool to detect different biomarkers in physiological matrices. Future works will focus on the optimization of the assays in real patient matrices and to utilize the array layout of the sensors to detect various biomarkers in one assay, simultaneously.

Acknowledgments

This work was funded by the European Commission Program through the Marie Curie Initial Training Network PROSENSE (Grant no. 317420, 2012–2016, www.prosense-itn.eu). Vivek Pachauri thanks the Euroimmun AG and the Stiftung Rheinland-Pfalz für Innovation (Grant no. 1082) for funding of his position. The authors thank Detlev Cassel for his support in device fabrication and Rainer Lilischkis (both University of Applied Sciences Kaiserslautern, Germany) for his support with SEM imaging.

Supporting information

The supporting information file contains the full spectral range recordings of the in-line EIS experiments, the ISFET recordings of the rGO IDE sensors, characterizations of rGO thin films in dry conditions and recordings in a classical EIS configuration using both arms of the IDEs as WEs.

Appendix A. Supplementary material

Supplementary data associated with this article can be found in the online version at doi:10.1016/j.bios.2018.09.045.

References

Antenor, J.A.V., Roehl, K.A., Eggener, S.E., Kundu, S.D., Han, M., Catalona, W.J., 2005. Preoperative PSA and progression-free survival after radical prostatectomy for Stage T1c disease. Urology 66, 156–160. https://doi.org/10.1016/j.urology.2005.01.008.

Baade, P.D., Youlden, D.R., Krnjacki, L.J., 2009. International epidemiology of prostate cancer: geographical distribution and secular trends. Mol. Nutr. Food Res. https://doi.org/10.1002/mnfr.200700511.

Bagri, A., Mattevi, C., Acik, M., Chabal, Y.J., Chhowalla, M., Shenoy, V.B., 2010. Structural evolution during the reduction of chemically derived graphene oxide. Nat. Chem. 2, 581–587. https://doi.org/10.1038/nchem.686.

Baringhaus, J., Ruan, M., Edler, F., Tejeda, A., Sicot, M., Taleb-Ibrahimi, A., Li, A.-P., Jiang, Z., Conrad, E.H., Berger, C., Tegenkamp, C., de Heer, W.A., 2014. Exceptional ballistic transport in epitaxial graphene nanoribbons. Nature 506, 349–354.

Barsoukov, E., Macdonald, J.R., 2005. Impedance Spectroscopy: Theory, Experiment, and Applications, 2nd edition. Wiley, New Jersey, USA. https://doi.org/10.1002/0471716243.

Bart, M., Stigter, E.C.A., Stapert, H.R., De Jong, G.J., Van Bennekom, W.P., 2005. On the response of a label-free interferon-γ immunosensor utilizing electrochemical impedance spectroscopy. Biosens. Bioelectron. 21, 49–59. https://doi.org/10.1016/j.bios.2004.10.009.

Berdat, D., Marin, A., Herrera, F., Gijs, M.A.M., 2006. DNA biosensor using fluorescence microscopy and impedance spectroscopy. Sens. Actuators B Chem. 118, 53–59. https://doi.org/10.1016/j.snb.2006.04.064.

Berdat, D., Rodríguez, A.C.M., Herrera, F., Gijs, M.A.M., 2008. Label-free detection of DNA with interdigitated micro-electrodes in a fluidic cell. Lab Chip 8, 302–308. https://doi.org/10.1039/B712609C.

Bonanni, A., Ambrosi, A., Pumera, M., 2012a. Nucleic acid functionalized graphene for biosensing. Chem. - A Eur. J. 18, 1668–1673. https://doi.org/10.1002/chem.201102850.

Bonanni, A., Loo, A.H., Pumera, M., 2012b. Graphene for impedimetric biosensing. TrAC - Trends Anal. Chem. 37, 12–21. https://doi.org/10.1016/j.trac.2012.02.011.

Castro Neto, A.H., Guinea, F., Peres, N.M.R.M.R., Novoselov, K.S.S., Geim, A.K.K., 2009. The electronic properties of graphene. Rev. Mod. Phys. 81, 109–162. https://doi.org/10.1103/RevModPhys.81.109.

De, S., Coleman, J.N., 2010. Are there fundamental limitations on the sheet resistance and transmittance of thin graphene films? ACS Nano 4, 2713–2720. https://doi.org/10.1021/nn100343f.

Dreyer, D.R., Park, S., Bielawski, C.W., Ruoff, R.S., 2010. The chemistry of graphene oxide. Chem. Soc. Rev. 39, 228–240. https://doi.org/10.1039/B917103G.

Eda, G., Chhowalla, M., 2010. Chemically derived graphene oxide: towards large-area thin-film electronics and optoelectronics. Adv. Mater. 22, 2392–2415.

Formisano, N., Jolly, P., Bhalla, N., Cromhout, M., Flanagan, S.P., Fogel, R., Limson, J.L., Estrela, P., 2015. Optimisation of an electrochemical impedance spectroscopy aptasensor by exploiting quartz crystal microbalance with dissipation signals. Sens. Actuators B Chem. 220, 369–375. https://doi.org/10.1016/j.snb.2015.05.049.

Geim, A.K., Novoselov, K.S., 2007. The rise of graphene. Nat. Mater. 6, 183–191.

Gómez-Navarro, C., et al., 2007. Electronic transport properties of individual chemically reduced graphene oxide sheets. Nano Lett. 7, 3499–3503.

Huang, P.Y., Ruiz-Vargas, C.S., van der Zande, A.M., Whitney, W.S., Levendorf, M.P., Kevek, J.W., Garg, S., Alden, J.S., Hustedt, C.J., Zhu, Y., Park, J., McEuen, P.L., Muller, D.A., 2011. Grains and grain boundaries in single-layer graphene atomic patchwork quilts. Nature 469, 389–392.

Igreja, R., Dias, C.J., 2004. Analytical evaluation of the interdigital electrodes capacitance for a multi-layered structure. Sens. Actuators A Phys. 112, 291–301.

Jolly, P., Formisano, N., Tkáč, J., Kasák, P., Frost, C.G., Estrela, P., 2015. Label-free impedimetric aptasensor with antifouling surface chemistry: a prostate specific antigen case study. Sens. Actuators B Chem. 209, 306–312. https://doi.org/10.1016/j.snb.2014.11.083.

Kahng, Y.H., Lee, S., Park, W., Jo, G., Choe, M., Lee, J.-H., Yu, H., Lee, T., Lee, K., 2012. Thermal stability of multilayer graphene films synthesized by chemical vapor deposition and stained by metallic impurities. Nanotechnology 23, 75702. https://doi.org/10.1088/0957-4484/23/7/075702.

Lanche, R., Pachauri, V., Koppenhöfer, D., Wagner, P., Ingebrandt, S., 2014. Reduced graphene oxide-based sensing platform for electric cell-substrate impedance sensing. Phys. Status Solidi Appl. Mater. Sci. 211, 1404–1409. https://doi.org/10.1002/pssa.201330522.

Liang, X., Sperling, B.A., Calizo, I., Cheng, G., Hacker, C.A., Zhang, Q., Obeng, Y., Yan, K., Peng, H., Li, Q., Zhu, X., Yuan, H., Walker, A.R.H., Liu, Z., Peng, L., Richter, C.A., 2011. Toward clean and crackless transfer of graphene. ACS Nano 5, 9144–9153.

Lisdat, F., Schafer, D., 2008. The use of electrochemical impedance spectroscopy for biosensing. Anal. Bioanal. Chem. 391, 1555–1567. https://doi.org/10.1007/s00216-008-1970-7.

Lu, X., Munief, W.-M., Heib, F., Schmitt, M., Britz, A., Grandthyl, S., Müller, F., Neurohr, J.-U., Jacobs, K., Benia, H.M., Lanche, R., Pachauri, V., Hempelmann, R., Ingebrandt, S., 2018. Front-end-of-line integration of graphene oxide for graphene-based electrical platforms. Adv. Mater. Technol. 1700318, 1700318. https://doi.org/10.1002/admt.201700318.

Macdonald, J.R., 2005. Impedance spectroscopy: models, data fitting, and analysis. Solid State Ion. 176, 1961–1969. https://doi.org/10.1016/j.ssi.2004.05.035.

Macdonald, J.R., 1990. Impedance spectroscopy: old problems and new developments. Electrochim. Acta 35, 1483–1492. https://doi.org/10.1016/0013-4686(90)80002-6.

Munief, W.-M., Heib, F., Hempel, F., Lu, X., Schwartz, M., Pachauri, V., Hempelman, R., Schmitt, M., Ingebrandt, S., 2018a. Silane deposition via gas-phase evaporation and high-resolution surface characterization of the ultrathin siloxane coatings. Langmuir. https://doi.org/10.1021/acs.langmuir.8b01044. (Published online).

Munief, W.-M., Lu, X., Teucke, T., Wilhelm, J., Britz, A., Hempel, F., Schwartz, M., Law, J. K.Y., Lanche, R., Grandthyll, S., Müller, F., Neurohr, J.-U., Jacobs, K., Schmitt, M., Hempelmann, R., Pachauri, V., Ingebrandt, S., 2018b. Reduced graphene oxide biosensor platform for the detection of NT-proBNP biomarker in its clinical range. (Submitted for publication).

Novoselov, K.S., Fal'ko, V.I., Colombo, L., Gellert, P.R., Schwab, M.G., Kim, K., 2012. A roadmap for graphene. Nature 490, 192–200. https://doi.org/10.1038/nature11458.

Novoselov, K.S., Geim, A.K., Morozov, S.V., Jiang, D., Zhang, Y., Dubonos, S.V., Grigorieva, I.V., Firsov, A.A., 2004. Electric field effect in atomically thin carbon films. Science 306, 666–669. https://doi.org/10.1126/science.1102896.

Orazem, M.E., Tribollet, B., 2011. Electrochemical Impedance Spectroscopy. Wiley, New Jersey, USA. https://doi.org/10.1002/9780470381588.

Pei, S., Cheng, H.-M.M., 2012. The reduction of graphene oxide. Carbon N.Y. 50, 3210–3228. https://doi.org/10.1016/j.carbon.2011.11.010.

Rani, D., Pachauri, V., Madaboosi, N., Jolly, P., Vu, X.-T., Estrela, P., Chu, V., Conde, J.P., Ingebrandt, S., 2018. Top-down fabricated silicon nanowire arrays for field-effect detection of prostate-specific antigen. ACS Omega 3 (8), 8471–8482.

Schmitt, M., 2014. Analysis of silanes and of siloxanes formation by Raman spectroscopy.

RSC Adv. 4, 1907–1917. https://doi.org/10.1039/C3RA45306E.
Schmitt, M., Hempelmann, R., Ingebrandt, S., Munief, W.-M., Gross, K., Grub, J., Heib, F., 2015. Statistical approach for contact angle determination on inclining surfaces: “slow-moving” analyses of non-axisymmetric drops on a flat silanized silicon wafer. J. Adhes. Sci. Technol. 29, 1796–1806. https://doi.org/10.1080/01694243.2014.976000.
Suk, J.W., Kitt, A., Magnuson, C.W., Hao, Y., Ahmed, S., An, J., Swan, A.K., Goldberg, B.B., Ruoff, R.S., 2011. Transfer of CVD-grown monolayer graphene onto arbitrary substrates. ACS Nano 5, 6916–6924.
Yang, L., Li, Y., Erf, G.F., 2004. Interdigitated array microelectrode-based electrochemical impedance immunosensor for detection of Escherichia coli O157:H7. Anal. Chem. 76, 1107–1113. https://doi.org/10.1021/ac0352575.
Zaretsky, M.C., Mouayad, L., Melcher, J.R., 1988. Continuum properties from interdigital electrode dielectrometry. Electr. Insul. IEEE Trans. 23, 897–917.